Vertical Vibrations of the Vehicle Excited by Ride Test

Massimo Cavacece, Giorgio Figliolini, and Chiara Lanni

1 Introduction

The influence of a rough road surface on vehicle vertical vibrations and on the driver and passengers is an important research among automotive manufacturers [3]. ISO international standard defines the terminology of vehicle dynamics and road-holding ability. In addition, ISO international standard proposes the test procedures for steady-state circular driving behavior and lateral transient response characteristics against step steering input, sinusoidal steering input, random steering input, and braking in a turn [6]. The standardized test procedure of a double-lane-change test as a severe lane-change maneuver is proposed [2]. In order to estimate the influence of vertical vibration on seated human body, the apparent mass of the human body is evaluated by mechanical lumped models [4]. In this research, a mechanical equivalent model has been developed to characterize the response of the vehicle excited by road profiles. The mechanical equivalent model offers a quantitative evaluation of accelerations of vehicle along vertical axis in terms of natural frequencies and dissipative properties of vehicle. In order to calibrate the mathematical model, an experimental design has been developed by the ride test.

M. Cavacece (✉) · G. Figliolini · C. Lanni
Department of Civil and Mechanical Engineering, University of Cassino and Southern Lazio, Cassino, Italy
e-mail: cavacece@unicas.it
URL: https://www.unicas.it/

Y. V. D. Rao et al. (eds.), *Advances in Industrial Machines and Mechanisms*,
Lecture Notes in Mechanical Engineering,
https://doi.org/10.1007/978-981-16-1769-0_57

2 Suspension System

The mass m_s represents the suspended mass (equal to a quarter of the mass of the entire vehicle) (Fig. 1). The unsprung mass associated with the suspension-wheel system is m_u. The variables z_s and z_u represent, respectively, the displacements, with respect to a horizontal reference axis, of the center of gravity of the suspended and unsprung mass. The quantity z_r describes the profile of the road surface. The stiffness constant k_u represents the elasticity of tire. The parameters k_s and c_s are, respectively, the elastic constant and the damping coefficient of the part passive suspension. The rest lengths of the corresponding springs are L_s and L_W. The force generated by the actuator between the wheel and the vehicle is $F(t)$ [1]. The g term is the acceleration of gravity. Model suspension system is described by the following equations:

$$\begin{aligned} m_s\ddot{z}_s(t) &= k_s[z_u(t) - z_s(t)] + c_s[\dot{z}_s(t) - \dot{z}_s(t)] + k_s L_s - m_s g + F(t) \\ m_u\ddot{z}_u(t) &= -k_s[z_u(t) - z_s(t)] + c_s[\dot{z}_s(t) - \dot{z}_s(t)] - k_s L_s \\ &\quad + k_u[z_r(t) - z_u(t)] + k_u L_u - m_u g - F(t)\ . \end{aligned} \tag{1}$$

From the equilibrium equations corresponding to the null values of z_r and F, we obtain

$$\begin{aligned} \bar{z}_s &= L_s + L_u - \left(\frac{m_s}{k_s} + \frac{m_s + m_u}{k_s}\right) g \\ \bar{z}_u &= L_u - \frac{(m_s + m_u)}{k_u} g\ . \end{aligned} \tag{2}$$

Equation (2) represents the positions of the center of gravity of the suspended mass and of the unsprung mass in static conditions, under the action of gravity. The following notation is introduced:

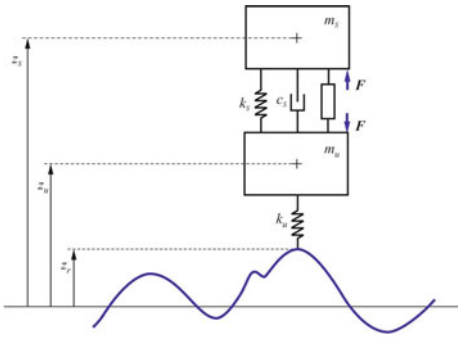

Fig. 1 Vehicle suspension system

$$\begin{aligned}\delta z_s(t) &= z_s(t) - \bar{z}_s,\\ \delta z_u(t) &= z_u(t) - \bar{z}_u\\ \delta z_r(t) &= z_r(t) - \bar{z}_r = z_r(t).\end{aligned} \tag{3}$$

We obtain the following system of equations:

$$\begin{aligned}m_s\delta\ddot{z}_s(t) &= k_s[\delta z_u(t) - \delta z_s(t)] + c_s[\delta\dot{z}_s(t) - \delta\dot{z}_s(t)] + F(t)\\ m_u\delta\ddot{z}_u(t) &= -k_s[\delta z_u(t) - \delta z_s(t)] - c_s[\delta\dot{z}_s(t) - \delta\dot{z}_s(t)]\\ &\quad + k_u[\delta z_r(t) - \delta z_u(t)] - F(t)\ .\end{aligned} \tag{4}$$

State vectors are defined

$$x(t) = \begin{Bmatrix}\delta z_s(t)\\ \delta z_u(t)\\ \delta\dot{z}_s(t)\\ \delta\dot{z}_u(t)\end{Bmatrix}, \qquad u(t) = \begin{Bmatrix}\delta z_r(t)\\ F(t)\end{Bmatrix}. \tag{5}$$

The equations become

$$\dot{\boldsymbol{x}} = \boldsymbol{A}\boldsymbol{x}(t) + \boldsymbol{B}\boldsymbol{u}(t)\ , \tag{6}$$

with

$$\boldsymbol{A} = \begin{bmatrix}0 & 0 & 1 & 0\\ 0 & 0 & 0 & 1\\ -\dfrac{k_s}{m_s} & \dfrac{k_s}{m_s} & -\dfrac{c_s}{m_s} & \dfrac{c_s}{m_s}\\ \dfrac{k_s}{m_u} & -\dfrac{(k_s+k_u)}{m_s} & \dfrac{c_s}{m_s} & -\dfrac{c_s}{m_s}\end{bmatrix}, \qquad \boldsymbol{B} = \begin{bmatrix}0 & 0\\ 0 & 0\\ 0 & \dfrac{1}{m_s}\\ \dfrac{k_u}{m_u} & -\dfrac{1}{m_u}\end{bmatrix}. \tag{7}$$

The model's output variables are the vertical acceleration of the vehicle $a_s(t)$ and the variation of the contact force between the wheel and the road with respect to the force value static contact:

$$\delta F_c(t) = F_c(t) - \bar{F}_c = k_u[\delta z_u(t) - \delta z_r(t)]\ . \tag{8}$$

with $\bar{F}_c = (m_s + m_u)g$. We obtain

$$y(t) = \begin{Bmatrix}a_s(t)\\ \delta F_c(t)\end{Bmatrix} = \boldsymbol{C}\boldsymbol{x}(t) + \boldsymbol{D}\boldsymbol{u}(t) \tag{9}$$

with

$$\boldsymbol{C} = \begin{bmatrix} -\frac{k_s}{m_s} & \frac{k_s}{m_s} & -\frac{c_s}{m_s} & \frac{c_s}{m_s} \\ 0 & k_u & 0 & 0 \end{bmatrix} \quad \boldsymbol{D} = \begin{bmatrix} \frac{1}{m_s} & 0 \\ 0 & -k_u \end{bmatrix}. \tag{10}$$

Equation (10) constitutes a state-space representation of the system. The dynamic system is invariant not strictly proper, of order 4, with two inputs and two outputs (MIMO system model). The first input can be seen as a disturbance, while the second is the control variable.

3 Open-Loop Transfer Functions

Considering the open loop, the inputs are δz_r and F and outputs are a_s and δF_c [1]. The transfer functions between the two inputs and the two outputs are the following relations:

$$\begin{aligned} G_{11}(s) &= \frac{A_s(s)}{Z_r(s)} = \frac{\mu_{11} s^2 (1 + s\tau_1)}{\left(1 + \frac{2\xi_1 s}{\omega_{n1}} + \frac{s^2}{\omega_{n1}^2}\right)\left(1 + \frac{2\xi_2 s}{\omega_{n2}} + \frac{s^2}{\omega_{n2}^2}\right)} \\ G_{12}(s) &= \frac{A_s(s)}{F(s)} = \frac{\mu_{12} s^2 \left(1 + \frac{s^2}{\alpha_{n1}^2}\right)}{\left(1 + \frac{2\xi_1 s}{\omega_{n1}} + \frac{s^2}{\omega_{n1}^2}\right)\left(1 + \frac{2\xi_2 s}{\omega_{n2}} + \frac{s^2}{\omega_{n2}^2}\right)} \\ G_{21}(s) &= \frac{F_c(s)}{Z_r(s)} = \frac{\mu_{21} s^2 (1 + s\tau_1)(1 + s\tau_2)}{\left(1 + \frac{2\xi_1 s}{\omega_{n1}} + \frac{s^2}{\omega_{n1}^2}\right)\left(1 + \frac{2\xi_2 s}{\omega_{n2}} + \frac{s^2}{\omega_{n2}^2}\right)} \\ G_{22}(s) &= \frac{F_c(s)}{Z_r(s)} = \frac{\mu_{22}}{\left(1 + \frac{2\xi_1 s}{\omega_{n1}} + \frac{s^2}{\omega_{n1}^2}\right)\left(1 + \frac{2\xi_2 s}{\omega_{n2}} + \frac{s^2}{\omega_{n2}^2}\right)}. \end{aligned} \tag{11}$$

There are two resonance conditions for the system: one at ω_{n_1} and another at ω_{n_2}. The damping factors associated with the conjugated complex pole pairs are low values. In addition, the functions $G_{11}(s)$, $G_{12}(s)$, $G_{21}(s)$, and $G_{22}(s)$ contain a double derivative action.

The effect of the road profile on vertical acceleration is analyzed, in the absence of control actions. Figure 3 shows the Bode diagram of the magnitude of the $G_{11}(s)$ transfer function. The values of the transfer function $G_{11}(s)$ show high values in the medium- to high-frequency range. The transfer function $G_{11}(s)$ peaks at the natural frequency ω_{n2}. An effective suspension system mitigates the values of peaks.

The vehicle is equipped with passive suspension. Vehicle speed is $v = 10$ km/h $\cong$ 2.8 m/s on a rectangular bump. Table 1 shows input data of mathematical modeling and simulation. The profile of the bump is shown in Fig. 2.

The wheel hits the bump at $t = 1$ s. The wheel leaves the bump at $t = 3$ s. Figure 4 shows the time trends of vertical acceleration and contact force caused by the bump profile. If the road profile presents an irregular appearance, described by a random

Fig. 2 Ride test

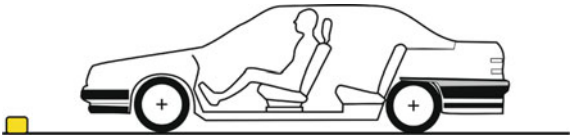

Fig. 3 Bode diagram

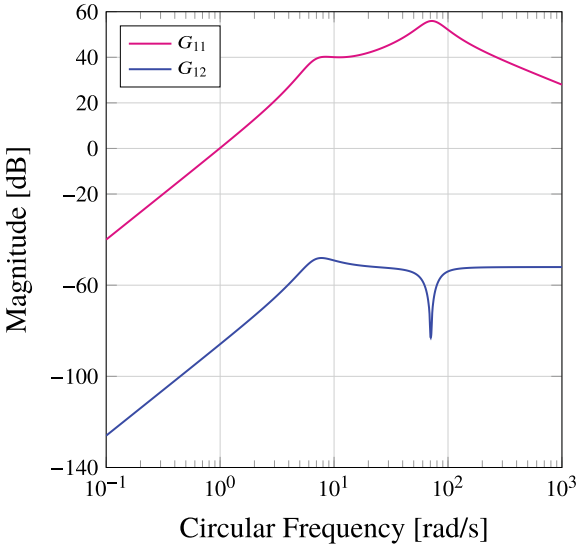

sign, the trends of accelerations and forces in time domain are proposed in Fig. 5. The Bode diagrams of the function $G_{12}(s)$ express the effect of the input $F(t)$ on the vertical acceleration (Fig. 3).

Two zeros at 0 Hz increase the transfer function $G_{11}(s)$ from 0 to 7 rad/s. Zero at about 10.0 rad/s of the transfer function $G_{11}(s)$ generates 40 dB from 6.92 rad/s to 14 rad/s (Table 2).

4 Experimental Design

In order to evaluate ride performance (Fig. 2), an accelerometer is attached at vehicle floor as shown in figure. An Axivity 6-axis accelerometer is used to measure the vibrations of six components of acceleration at a vehicle floor. The vertical component of the acceleration is utilized. The frequency range is from 0.5 to 1000 rad/s. A rectangular-shaped cleat bar on a road, shown in Fig. 2, is chosen for an impact object driving test [5]. The height and width of rectangular-shaped cleat bar are, respectively, 20 and 20 mm. The test speed is constant at 50 kph while front and rear tires are passing over the cleat bar. The experimental investigations consider the vertical vibrations of the elegant car during four ride tests (Figs. 6, 7, 8, 9, 10, 11,

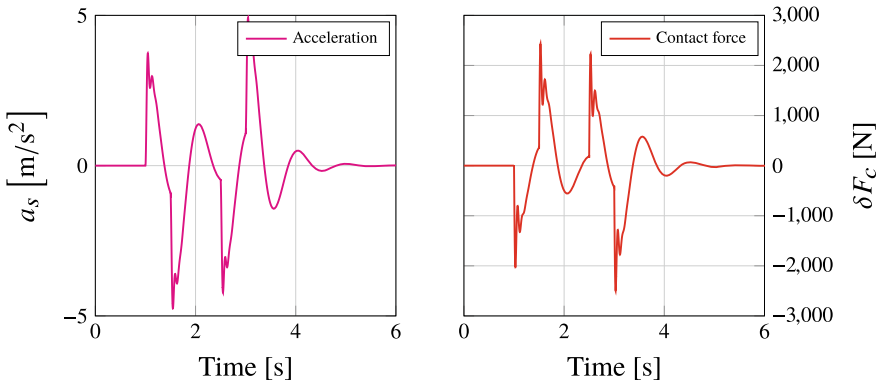

Fig. 4 Vertical accelerations of mass m_s and contact forces of open-loop system with rectangular bump ($v = 10$ km/h)

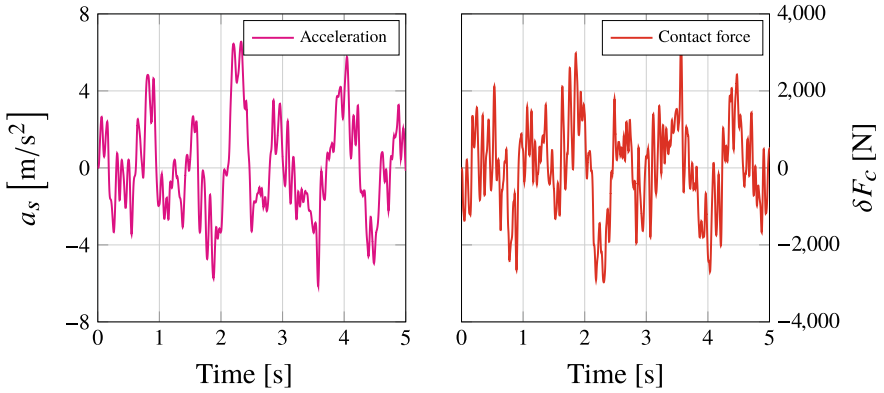

Fig. 5 Vertical accelerations of mass m_s and contact forces of open-loop system with random sign ($v = 10$ km/h)

12, and 13). The car is excited by road profiles. The time interval after impact is considered to estimate the vertical vibrations of vehicle.

5 Discussion

The impact object driving test characterizes the vehicle running over various impact objects. The frequencies of impact ranges from 1.5 to 50 Hz. Experimental investigations indicate relevant movements of the human body during vibration in the range from 4.5 to 7 Hz [5]. The vertical components of accelerations are obtained by ride test. The seat-rail vibrations are analyzed in terms of vertical components of accelerations in time and frequency domains (Figs. 6, 7, 8, 9, 10, 11, 12, and

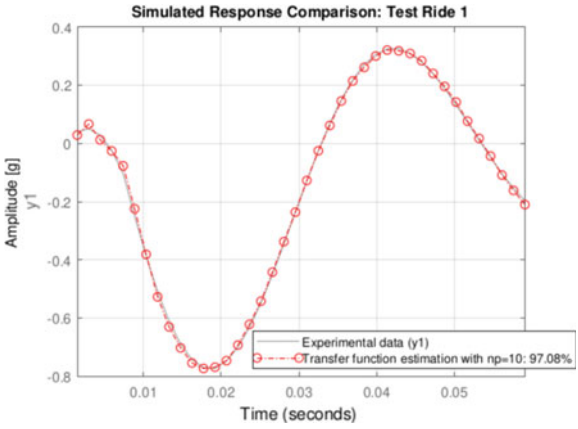

Fig. 6 Vertical accelerations of mass m_s during Ride Test 1 in time domain

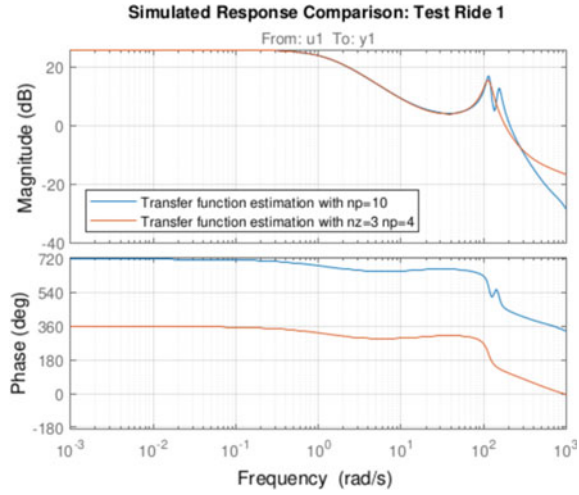

Fig. 7 Vertical accelerations of mass m_s during Ride Test 1 in frequency domain

13). The comparison between acceleration values obtained by mathematical model and ones obtained by experimental investigation is shown in Figs. 6, 8, 10, and 12. The comparison offers a good agreement (84–99%) between acceleration values obtained by mathematical model and ones obtained by experimental investigation in time domain. The mathematical simulation and the experimental investigation concern short and single impact test. The circular frequencies of vertical accelerations of vehicle excited by ride tests lie in three different regions 0–10, 10–20, and 20–80 [rad/s] (Figs. 7, 9, 11, and 13).

If rear tires are passing over the cleat bar, the peak value of the vertical component of vehicle increases. After the impact of rear tires, the vertical component is not easily damped out. One reason for the low damping is that the irregularities of road profile excite the vehicle after the impact between a vehicle and a rectangular-shaped cleat

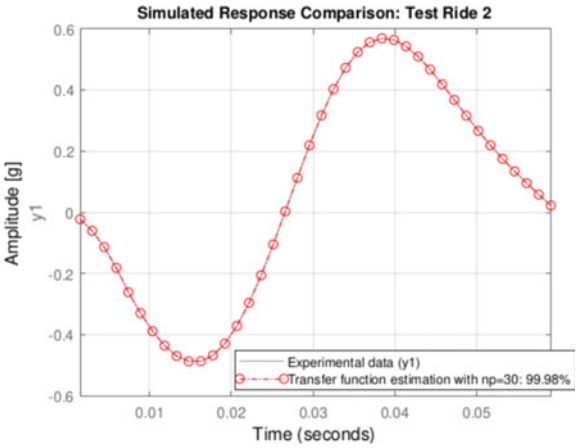

Fig. 8 Vertical accelerations of mass m_s during Ride Test 1 in time domain

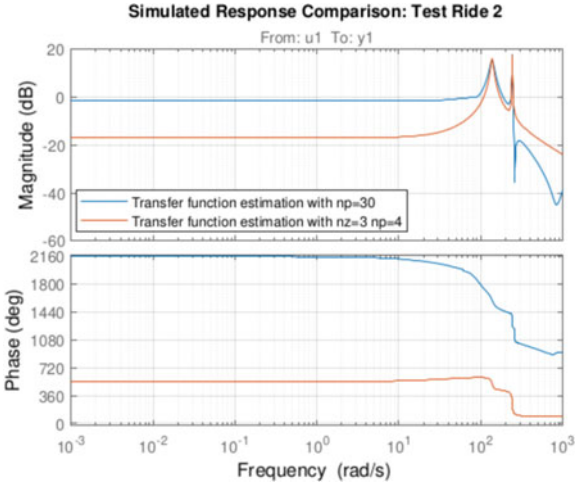

Fig. 9 Vertical accelerations of mass m_s during Ride Test 1 in frequency domain

bar on a road. Figure 14 illustrates damping ratio versus damped frequencies of the vehicle evaluated by ride test.

Table 3 shows the values of the composite weighted level and the fourth power vibration dose VDV for ride test ($v = 50$ km/h).

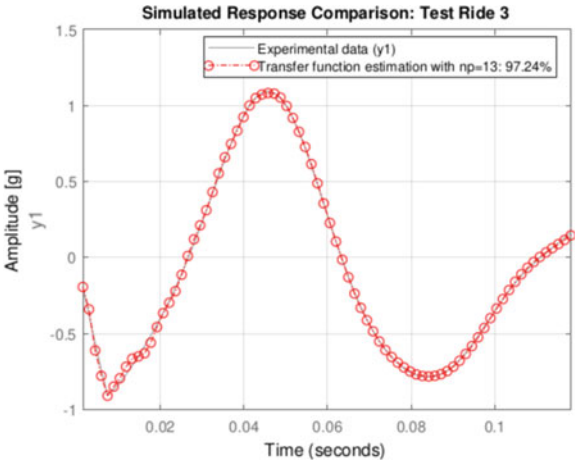

Fig. 10 Vertical accelerations of mass m_s during Ride Test 2 in frequency domain

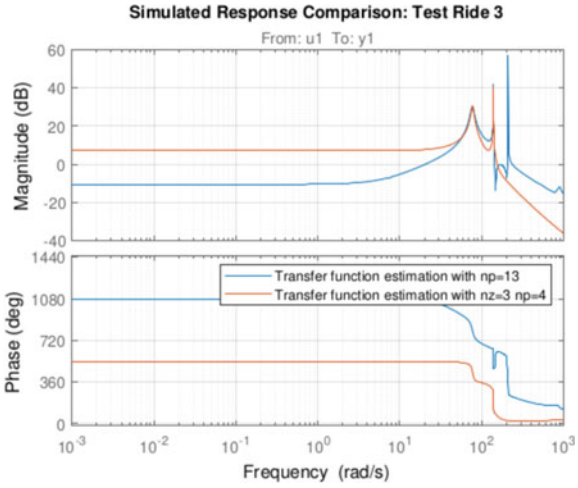

Fig. 11 Vertical accelerations of mass m_s during Ride Test 3 in time domain

Table 1 Input data

Symbol	Description	Numerical value
m_s	Suspended mass	400 [kg]
m_u	Unsprung mass	50 [kg]
k_u	Elasticity of tire	$2.5 \cdot 10^5$ [N/m]
k_s	Stiffness coefficient of the passive suspension	$2 \cdot 10^4$ [N/m]
c_s	Damping coefficient of the passive suspension	$2 \cdot 10^3$ [Nsm^{-1}]

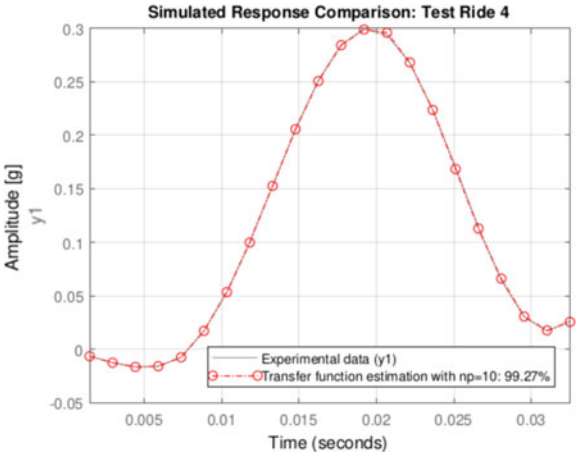

Fig. 12 Vertical accelerations of mass m_s during Ride Test 3 in frequency domain

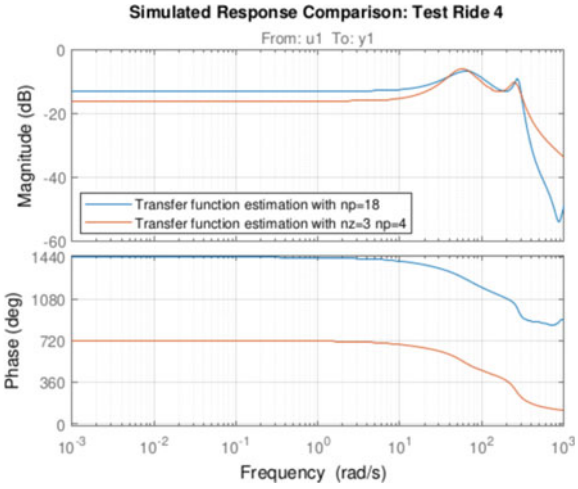

Fig. 13 Vertical accelerations of mass m_s during Ride Test 4 in time domain

Table 2 Natural frequencies, damping ratio, zeros, gain, and time constant of function G_{11}

Zero	Pole	Damping ratio	Frequency [rad/s]	Time constant [s]
0	$-2.21 \pm i6.56$	0.32	6.92	0.453
-10	$-20.30 \pm i69.40$	0.28	72.30	0.05

Table 3 Composite weighted level AW, fourth power vibration dose VDV for ride test ($v = 50$km/h)

Description ride test	ID	AW $[\mathrm{m} \cdot \mathrm{s}^2]$	VDV $[\mathrm{m} \cdot \mathrm{s}^{1.75}]$
	1	0.7698	0.6652
	2	0.6432	0.5225
	3	2.376	1.864
	4	0.825	0.6688

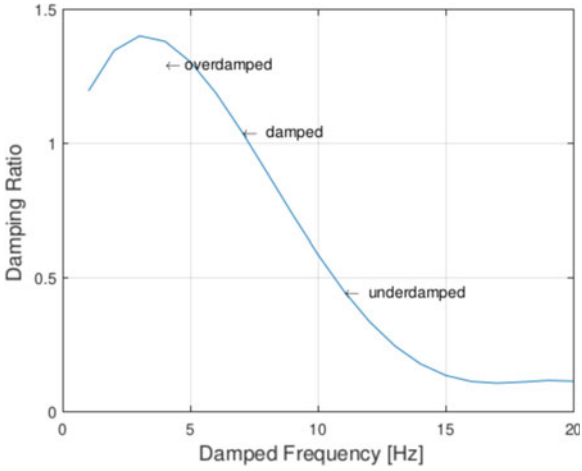

Fig. 14 Damping versus damped frequencies

Table 4 Symbols

Symbol	Description
m_s	Suspended mass
m_u	Unsprung mass
nz	Zeros
np	poles
z_s	Displacements of the center of gravity
z_u	Displacement of unsprung mass
z_r	Profile of the road surface
k_u	Elasticity of tire
k_s	Stiffness coefficient of the passive suspension
c_s	Damping coefficient of the passive suspension
L_s, L_W	Rest lengths of the corresponding springs
F	Force generated by the actuator
g	Acceleration of gravity
v	Vehicle speed

6 Conclusion

A mechanical equivalent model has been developed to characterize the response of the vehicle excited by road profiles. The mathematical model is calibrated by the ride test. During the tests, the accelerations represent objective measurement variables to illustrate the vehicle motion variables. The subjective assessment variables can be represented in mathematical formulation. Physical perception variables are related to the vehicle motion variables.

References

1. Bolzern, P., Scattolini, R., Schiavoni, N.: Fondamenti di Controlli Automatici. McGraw-Hill, Milano, Italy (2008)
2. ISO, Mechanical vibration and shock: Evaluation of human exposure to whole-body vibration. International Standard, ISO 2631-1:2014, 2014
3. Mastinu, G., Ploechl, M.: Road and Off–Road Vehicle System Dynamics, CRC Press (2014)
4. Cavacece, M., Pennestri, E.: Three degree of freedom model for the apparent mass of the seated human body exposed to vertical vibration. In: 51th UK Conference on Human Response to Vibration, Institute of Naval Medecine Gosport (2016). ISBN 978-0-9546028, 19
5. Aghilone, G., Cavacece, M.: Vibration Transmission performance of off-road vehicle seats. In: 53th UK Human Response Vibration, Ascot (UK), pp. 201–208 (2018)
6. Figliolini, G., Lanni, C., Angeles, J.: Kinematic analysis of the planar motion of vehicles when traveling along tractrix curves. ASME. J. Mech. Robot. **12**(5), 054502 (2020). https://doi.org/10.1115/1.4046509